DOI 10.1007/s11106-019-00010-1
Powder Metallurgy and Metal Ceramics, Vol. 57, Nos. 9-10, January, 2019 (Russian Original Vol. 57, Nos. 9-10, Sept.-Oct., 2018)

THEORY AND TECHNOLOGY OF SINTERING, THERMAL AND THERMOCHEMICAL TREATMENT

PRESSURELESS SPARK PLASMA SINTERING: A PERSPECTIVE FROM CONVENTIONAL SINTERING TO ACCELERATED SINTERING WITHOUT PRESSURE

R. Yamanoglu[1]

UDC 621.762.5

Spark plasma sintering (SPS) has been an attractive technique for many researchers seeking to consolidate metals and ceramics. This technique's high heating rates with the support of simultaneous applied pressure result in highly densified materials. One of the most important effects of a high heating rate is the limitation of grain growth, which results in enhanced mechanical properties. Recently, a relatively new form of SPS with its own unique advantages was developed and is most commonly referred to as pressureless spark plasma sintering (PSPS). There has been an increase in the usage of this method in several applications such as porous material production, sintering of materials with a finer grain structure, and consolidation of green bodies in a short time. Although there have been many studies on PSPS, there is currently no review of the pressureless applications of SPS. This paper provides a link from SPS to PSPS and discusses the different applications in some detail.

Keywords: *powder metallurgy, spark plasma sintering, pressureless sintering, densification.*

INTRODUCTION

Powder metallurgy is preferred for different applications due to its advantages compared to conventional techniques. Complex shaped components with small dimensions can be easily controlled by powder metallurgy [1, 2]. Several historical perspectives of powder metallurgy have been reported by different authors [3–6]. Sintering of materials has a long history. Early civilizations began to build materials from powders to useful shapes using powder metallurgy. Gold, silver, copper, and iron powders were obtained by grinding and without melting subjected to heat for building materials. The most common examples for the earliest powder metallurgical parts are iron implants, coins, iron pillar of Delhi, daggers, etc. [7, 8]. Many examples have been shown by analysis of fired materials found in China, India, Egypt, Japan, Turkey, Korea, Central America, and Southern Europe. However, controlling the sintering process by different temperatures and holding times was started to produce sintered products in Spain, China, Korea, Japan, Germany, England, and Russia only a few hundred years ago [9].

[1]Kocaeli University, Department of Metallurgical and Materials Engineering, 41380, Kocaeli, Turkey; e-mail: ryamanoglu@gmail.com.

Published in Poroshkova Metallurgiya, Vol. 57, Nos. 9–10 (523), pp. 22–36, 2018. Original article submitted March 1, 2018.

For material processing using sintering, energy reduction is a vital issue. During the sintering process, the material's surface area is reduced by growing bonds at the contact points of nearby particles by means of heating. The exposed surface of neighboring particles is replaced by the formation of grain boundaries at the interparticle bonds, which are then removed by grain growth via densification. Therefore, the resulting grain size and density have a strong effect on the final properties of the sintered material. The grain growth and densification process are dependent on the sintering holding time and temperature and must be carefully controlled for optimal material properties [10].

Today, pressure-assisted sintering is helpful to enable enhanced material properties in different processed materials [11–15]. Applying high pressure to a compact powder during sintering causes a direct benefit to the densification and final mechanical properties of the material. External pressure has been found to enhance the densification rate reducing the required sintering temperature and holding time. These conditions have been observed to effectively suppress the rate of grain growth, which also results in improved mechanical properties [16]. The pressure effect can also be effective in the elimination of pores, and is usually used in tandem with a vacuum to improve the benefits from the densification step. Initially, sintering is performed under a vacuum to ensure a closed-pore condition with pores free of trapped gas. Afterwards, external pressure is applied to accelerate the elimination of the remained pores [17]. External pressure can be applied in one of the two ways: unidirectional or isostatic. Techniques using these approaches are defined as conventional pressure-assisted methods. Common methods include hot pressing (HP) for unidirectional application of pressure, and hot isostatic pressing (HIP) for isostatic pressure [18]. In HP procedures, loose powders are placed into a die, which is then placed between two punches and subjected to heat with simultaneous pressure. This operation may be conducted under vacuum or under a protective atmosphere. For uniaxial HP, graphite dies and punches are commonly preferred for their high thermal conductivity and self-lubrication properties. A graphite experimental setup is also suitable for inductive and resistive heating. In HIP procedures, however, flexible dies are used with hydrostatic pressurization. The powder compact is inserted through a threaded closure and pressure is applied by means of gas introduced to the chamber and any heating is performed after the gas is introduced [17–20].

Recently, there has been an increasing interest in current-activated sintering as a new pressure-assisted densification method due to the efficiency of the process and its ability to fabricate novel materials. By using a high electric current (ranges from ~1000 A to 10,000 A at 10–15 V maximum), it is possible to consolidate particles to a higher density faster than conventional sintering methods and hot pressing techniques [21]. Current-activated sintering techniques include many distinct methods, including spark plasma sintering (SPS), field-assisted sintering (FAST) [22, 23], pulsed electric-current-assisted sintering (PECAS) [24, 25], current-activated and pressure-assisted densification (CAPAD) [26, 27], electric-field-assisted sintering (EFAS) [28, 29], and pulsed electric current sintering (PECS) [30, 31]. Each method of current-assisted sintering is distinct due to their different process mechanisms [32]; however, the most common method is SPS and we will use it as a general term in the following sections.

SPARK PLASMA SINTERING

Figure 1 shows the number of academic papers related to SPS that have been published annually since 1994. The increasing trend can be clearly seen in the graph adapted from SCOPUS. In recent years, the SPS method has received a great deal of attention, with a large number of research studies and reviews completed describing applications of the technique. One of the most important commercial usage of the SPS technique is nuclear fuel pellets [33]. Other common applications of SPS are thermoelectric materials [34], biomaterials [35], and transparent materials [36]. Although there has been an increase in the usage of commercial SPS recently, the origin of current-activated sintering is much older. The method was first described in 1933 as a way to use an electric discharge or current to aid in the sintering of particles [37, 38]. Some sources also suggest that the earliest application of SPS began in 1906 when the first direct current (DC) resistance sintering apparatus was developed [39–41].

SPS has since been applied to the consolidation of different materials such as metals [42, 43], ceramics [44, 45], composites [46, 47], and functionally-graded materials [48, 49] with short processing times. To enable the

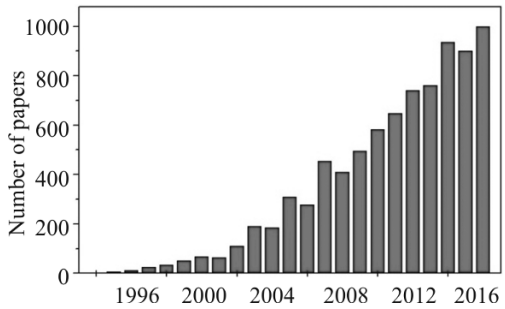

Fig. 1. Number of papers published on the spark plasma sintering of materials (adapted from SCOPUS)

innate advantage of short sintering times, SPS employs a spark discharge in the voids between particles and consolidates powders to near their full density. This spark discharge between neighboring particles activates the surfaces of each particle, purifies oxide contamination, and effectively self-heats the material. This effect also enables a lower required sintering temperature and shorter dwell times and often results in a denser structure with finer grain sizes and higher strength [50–52].

As a pressure-assisted sintering technique, SPS is in some ways similar to conventional HP techniques. However, the heating mechanisms of these two pressure-assisted sintering methods are very different. Heat is typically produced by a radiative furnace for HP methods, while SPS methods produce heat by Joule heating caused by an applied pulsed direct current of several thousand amperes and a few volts. The heating rate during SPS can reach up to 1000ºC/min. Similar to hot pressing, SPS often uses graphite molds as a die material. The applied uniaxial pressure during SPS is in the range of 10–100 MPa. These two effects consisting of high Joule heating rates and simultaneously applied pressure are the main causes of the enhanced densification enabled by SPS [53].

For conventional SPS methods, the effect and contribution of many different mechanisms have been studied, including plasma or microdischarge of the particles' surfaces, Joule heating, electromigration, local melting, and evaporation. One of the main issues focused on in these studies is the plasma effect between particles during sintering. Although there is some doubt about whether plasma forms between particles, there has not been any certain conclusion to be drawn. Many mechanisms for SPS and HP sintering have focused on the early stages of the sintering process. Most of them concluded that SPS enhances neck growth between particles and causes accelerated atomic diffusion compared to HP. However, there has thus far been relatively few investigations into the pressureless condition of SPS [54].

Based on the many advantages of the SPS method, a new approach called pressureless spark plasma sintering has been developed and used for a number of materials with different properties. Though this new pressureless form of SPS has drawn increasing amounts of attention recently, there has been no review published in this field. In the current review, we focused on the pressureless form of the SPS method.

PRESSURELESS SPARK PLASMA SINTERING

Pressureless spark plasma sintering (PSPS, also known as free pressureless spark plasma sintering) is a relatively novel modification of the conventional SPS method. Bradbury and Olevsky changed the conventional design assembly to enable a pressureless condition during SPS sintering. Their method used graphitic T-shaped punches instead of regular cylindrical punches. The working space remained constant between the fixed punch faces inside the standard SPS die resulting in zero external pressure during the sintering process. In both PSPS and SPS assemblies, contact resistance must be sufficient to provide resistance between the punch exteriors and die wall interiors. This resistance is vital for obtaining high temperatures and Joule heating rates during SPS. For this reason, graphite spacers are used at the contact point in the die design [55].

Several die designs showing a comparison between conventional and pressureless SPS are provided in Fig. 2. Guintini et al. detailed the process of PSPS and the heating mechanism can be summarized as follows: the

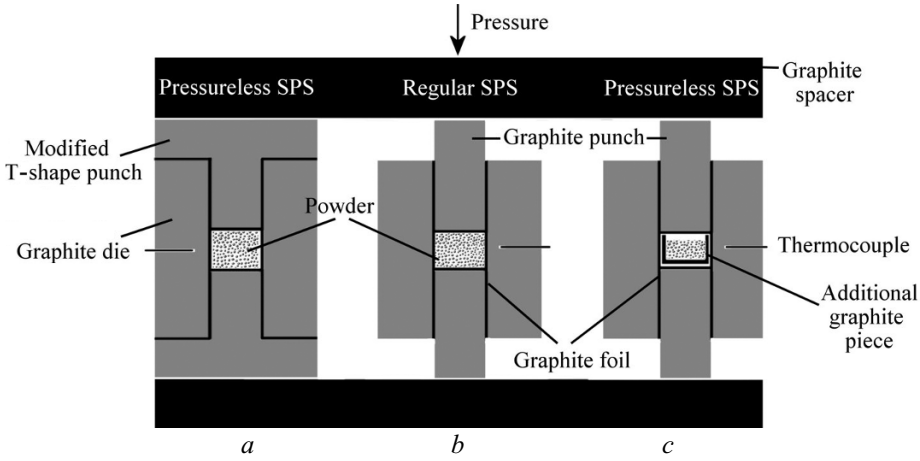

Fig. 2. Die designs of regular and pressureless SPS: *a*) pressureless form of SPS using T-shaped punches, *b*) regular SPS subjected to applied external pressure, and *c*) another form of pressureless SPS with an additional graphite piece [57]

electrical current goes from the T-shaped punch through the graphite die and causes an increase in the temperature of the die due to the Joule heating effect. This generated heat is transferred to the powder inside the die mainly by thermal conduction. The minimum load which is necessary for closing and maintaining the die assembly is sustained by the top and bottom surface of the two T-shaped punches, and thus the powder compact is not subjected to any external pressure [56].

Another form of PSPS was developed by Bertolla et al. Unlike the T-shaped punch used previously, they inserted an additional graphite piece inside a regular cylindrical SPS die assembly. This additional structural member was subjected to any minimum applied pressure and prevented it from affecting the sample [57].

Dudina et al. conducted a study on the evolution of spherical particle morphology in Al powders during PSPS. They did not observe any local melting or erosion for loosely packed Al powders sintered at 600ºC (Fig. 3). This is likely due to the high thermal conductivity of micrometer-sized metallic powders not sustaining the local interparticle overheating necessary for producing melting and necks [58].

In another study, although gross particle morphology did not change during sintering, Yamanoglu et. al. observed some local melting regions for a $Ti_5Al_{2.5}Fe$ alloy sintered by PSPS [59]. This observation can be attributed to the different temperature distribution from the particle surface through the core of the particle due to the applied pulsed electrical current. During sintering, the surface of the particle can reach its boiling point, resulting in enhanced neck formation between particles at relatively low temperatures by means of local melting areas [54, 60]. This effect is especially valid for highly porous structures. The electrical arc which occurs in the

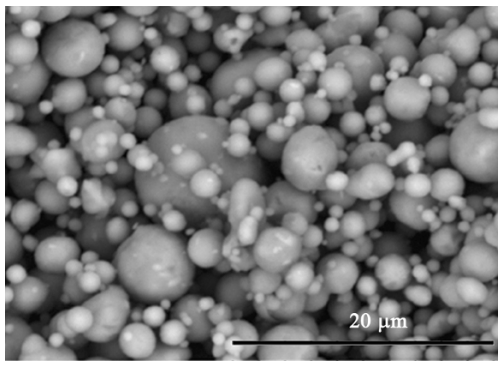

Fig. 3. The fracture surface of sintered loosely packed Al powders [58]

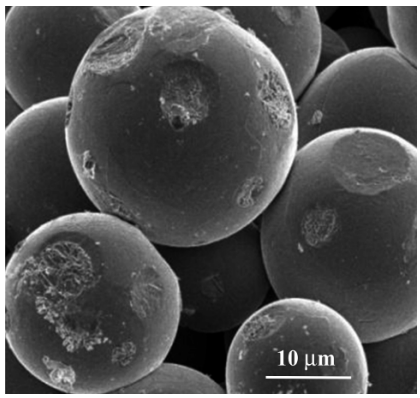

Fig. 4. Fracture surface of $Ti_5Al_{2.5}Fe$ alloy produced by pressureless spark plasma sintering [59]

pores between particles causes an extremely high temperature increase close to the neck points. The spherical particle shape remains largely unaffected, but the small plastically-deformed areas can be observed in Fig. 4 [59].

APPLICATION OF PRESSURELESS SPARK PLASMA SINTERING

Although the development of PSPS occurred relatively recently, there has been an increase in the usage of this method for several experimental aims. The usage of PSPS can be divided into three categories: prevention of grain growth by high heating rates for enhanced mechanical properties, production of a highly porous structure with controlled porosity ratio without applied pressure, and consolidation of green powder bodies within a short period.

PSPS is a suitable technique to enable densification of powder compacts previously shaped by different methods. Meng et al. used micro-powder injection molding (PIM) to obtain an alumina micro-channel compact and then densified it with PSPS. They successfully used PIM to obtain a fine and uniform microstructure while PSPS was then used to densify with high heating rates. Before the PSPS process, the powder binder was removed by thermal debinding and the micro-channel compact was placed into the PSPS assembly.

They attempted sintering with two different heating rates (100 and 200°C/min), and found that densification could not be achieved with a 200°C/min heating rate. In the study, the successful sintering conditions used was a temperature in the range of 1150 to 1350°C, a holding time of 5 min, and a 100°C/min heating rate. When the sintering temperature is increased in this range, the final density of the molded part increased. However, the authors observed that grain size increased abnormally at 1350°C resulting in a decrease of material hardness. This study proved that PIM-fabricated parts can be densified by PSPS with good shape retention and mechanical properties by inhibiting any grain coarsening effects [61].

Yamanoglu et al. successfully used PSPS for the production of porous biomedical titanium alloys. Prealloyed $Ti_5Al_{2.5}Fe$ powders were poured into the graphite die and T-shape punches were used to ensure a pressureless condition. Their sintering condition involved heating at 100°C/min to a final temperature in the range

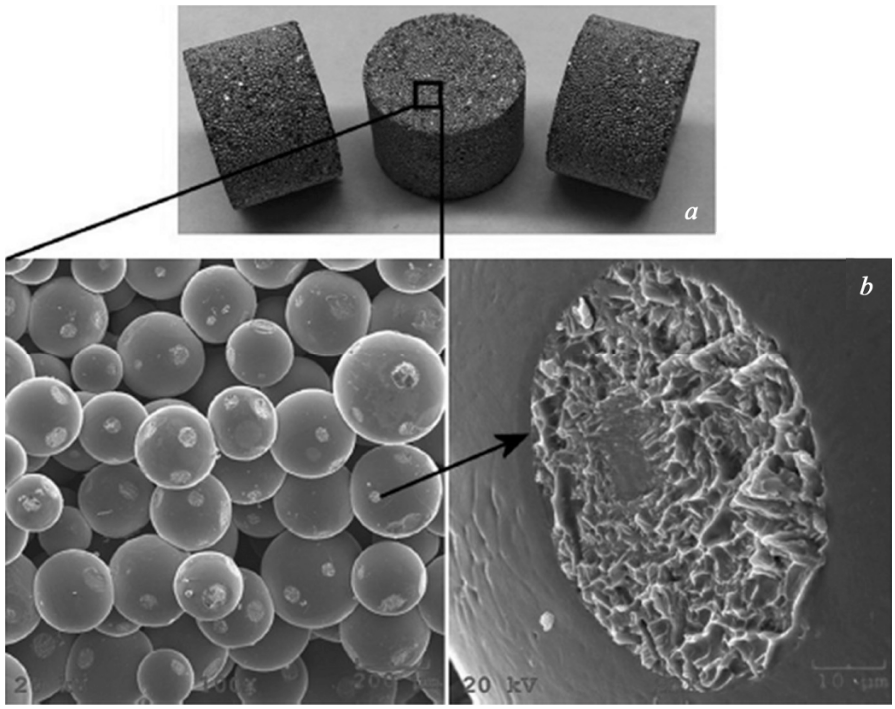

Fig. 5. PSPS-processed porous $Ti_5Al_{2.5}Fe$ alloy: *a*) macro image of porous compacts, *b*) SEM images of the porous structure with low and high magnification. No size and shape change is visible. The high heating rate is clear in the high magnification image of the particle contact point which resulted in stronger mechanical properties [59]

of 750–850°C for 5 min under vacuum atmosphere. In order to ensure the pulsed DC current reached between each particle, a minimum contact pressure of 5 MPa was applied. This pressure was maintained during the process to obtain a high heating rate effect on all of the interparticle contact points. In this regard, their application of SPS may be called partially pressureless SPS. The minimum pressure was applied to enable high heating rates, but further increase in the pressure was prevented by the T-shaped punches used during sintering. In regular PSPS, DC current heats the die and the powder is heated only through conduction. Despite the pressure applied, the authors did not observe any size or shape change in the particles after SPS processing. The obtained porosity ratios were 29.1, 28.7, and 28.4% for the sintering temperatures of 750, 800, and 850°C, respectively. Increased sintering temperature resulted in an increase in the final density. Figure 5 shows the porous titanium alloy obtained by PSPS using a T-shape punch [59].

Bradbury et al. produced SiC–C composites by PSPS using isolative zirconia felts and graphite paper spacers located between the die and punch faces to obtain a directed current path. They used three different heating rates (25, 50, and 100°C/min) to reach final sintering temperatures of 1300, 1500, and 1600°C with a holding time of 15 min. Contact pressure was maintained at 5 MPa throughout the process but was completely supported by the die rather than exerted on the powder. In their study, SiC nanowires with much greater aspect ratios, higher productivity, and straighter morphology were obtained using PSPS compared to other methods [55].

PSPS has also been successfully used for the sintering of bioactive glass powders. Bertolla et al. sintered commercial Bioglass 45S5 powder without pressure with a heating rate of 100°C/min and held at 1050°C for 30 min. They ensured a pressureless condition by using an additional graphite cup inside the regular SPS die assembly as shown in Fig. 2*c*. They placed cold isostatic pressed green bodies with a 13 mm diameter in a 20 mm die containing a supportive graphite cup with a greater height than the green bodies. Therefore, the minimal pressure of the regular SPS setup was supported by the additional graphite piece rather than the cold-pressed green bodies. In their study, PSPS-processed samples were compared with conventionally sintered samples (heat treated at 1050 °C with a heating rate of 5°C/min). The relative densities of the PSPS-treated samples were found to be higher than the conventionally sintered samples. The relative densities were 97.6% and 96.5% for PSPS treatment and conventionally sintered samples, respectively. The increase in density was found to be correlated with the higher heating rates in PSPS which overcame the second glass transition densification mechanism. The results were also supported by the observation that higher heating rates broadened the temperature range where viscous flow is not affected by the structural transformations of Bioglass. Besides the increased density, enhanced mechanical properties were also observed in PSPS-treated samples compared to conventional sintering. The superior mechanical properties were linked to the higher density values and fully crystalline fine microstructure of the PSPS-treated samples [57].

Lin et al. used a PSPS technique for the production of hydroxyapatite (HAP) microchannel structures. Aligned porous green bodies were fabricated from HAP slurries by dispersing HAP powder in deionized water followed by a freeze drying process. The HAP slurry was directionally frozen by means of a temperature gradient induced along a rubber tube which was placed on a copper rod dipped in liquid nitrogen. The directionally frozen green bodies were then processed by freeze drying at –50°C under 0.6 mbar pressure for 24 h. To prevent damage to the directional microchannel structures, PSPS was used for further processing at 1300°C for 1 h. They sintered the samples by PSPS successfully using an initial slurry concentrations of 15, 20, and 25 vol.%. Their results showed that the density and the compressive strength of the samples increased as the initial slurry concentration increased. The SEM images of the PSPS-treated samples after compression tests are shown in Fig. 6 [62].

A PSPS technique using a modified die to eliminate the pressure effect during sintering has also been used for the production of macroporous β-tricalcium phosphate scaffolds for the bone regeneration applications by Zhang et al. A mixture of β-tricalcium phosphate, polyethylene, and polyvinyl alcohol was pressed uniaxially into a 10 mm diameter and 8 mm thick puck, then heat treated at 400°C for 2 h. The compacts were presintered and inserted into the modified SPS die then sintered again at a temperature range of 850–1050°C for different times. They successfully controlled the porosity range of the compacts in the range of 55–70% with a macropore size of 300–500 μm. The grain growth of the nanocrystals was inhibited by means of high heating rates between the activated

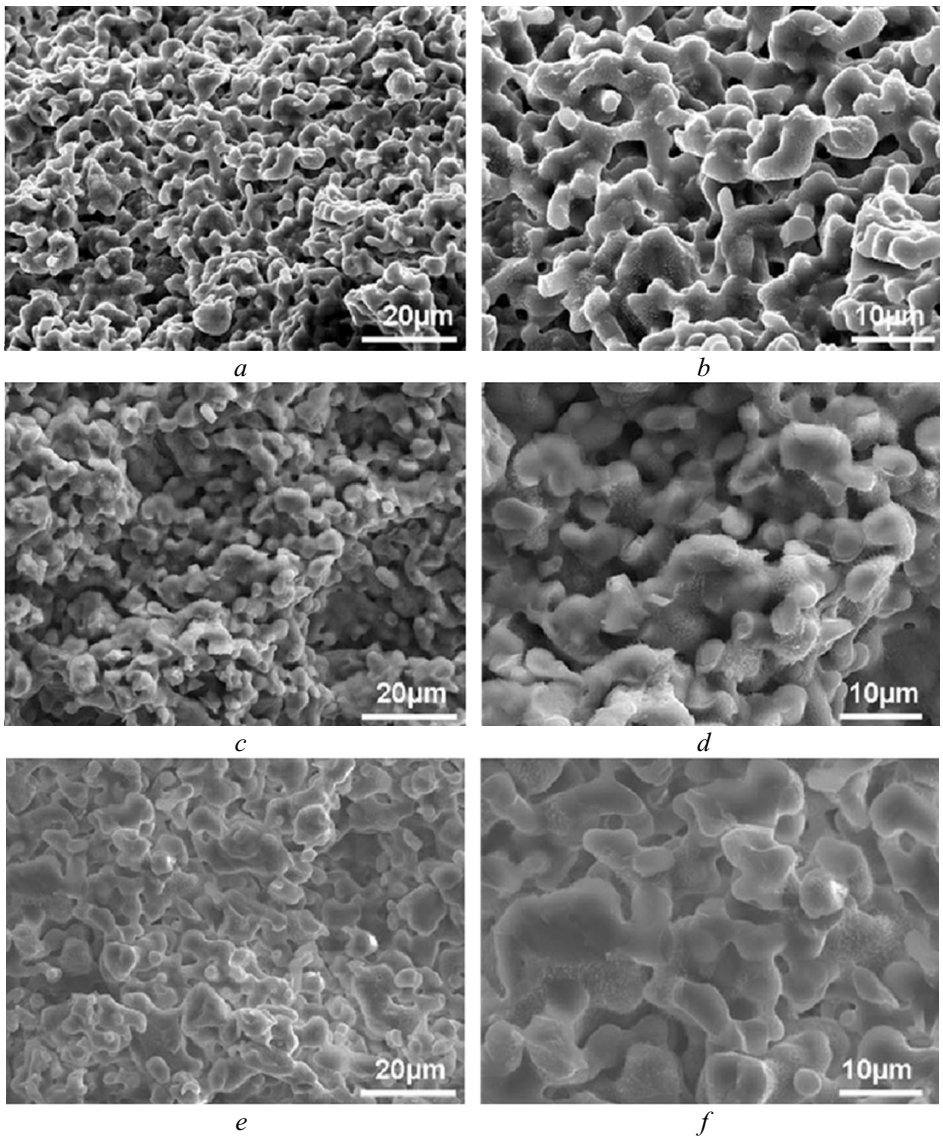

Fig. 6. SEM images of HAP samples with a significant amount of pores as a function of different slurry concentrations: *a–b*) 15%, *c–d*) 20%, and *e–f*) 25 vol.% slurry concentration [62]

nanoparticles causing enhanced diffusion during PSPS treatment. The SEM images of the macro-scaffolds compared to conventionally sintered samples are shown in Fig. 7 [63].

Quan et al. used PSPS treatment to produce Ti_6Al_4V foams by using a spaced holder die assembly. They used a conventional SPS setup to prepare a low-density pellet from a mixture of Ti_6Al_4V alloy and NaCl particles. Different weight ratios of NaCl particles were used to obtain different amounts of porosity. They reached a final temperature of 700°C and held the mixture for 8 min under 50 MPa of external pressure resulting in a disk with a 20 mm diameter and 5–7 mm thickness. The obtained disks with low densities had their NaCl content removed through dissolution in deionized water at room temperature. Following this treatment, PSPS was used as a post-heat treatment to ensure adequate consolidation. The PSPS treatment temperature and time were chosen to be 1100ºC and 5 min, respectively. The mixtures containing a different ratio of NaCl particles were placed into the SPS die and sintered at relatively low temperatures resulting in 47.6, 57.6, 63.9, and 72.5% porosities. When post-heat treated by PSPS at high temperature, the pellets had final porosities of 44.7, 54.4, 60.7, and 70.0%. Holding the pellets at high temperatures increased their density by 5.5, 7.5, 8.9, and 9.1%, respectively.

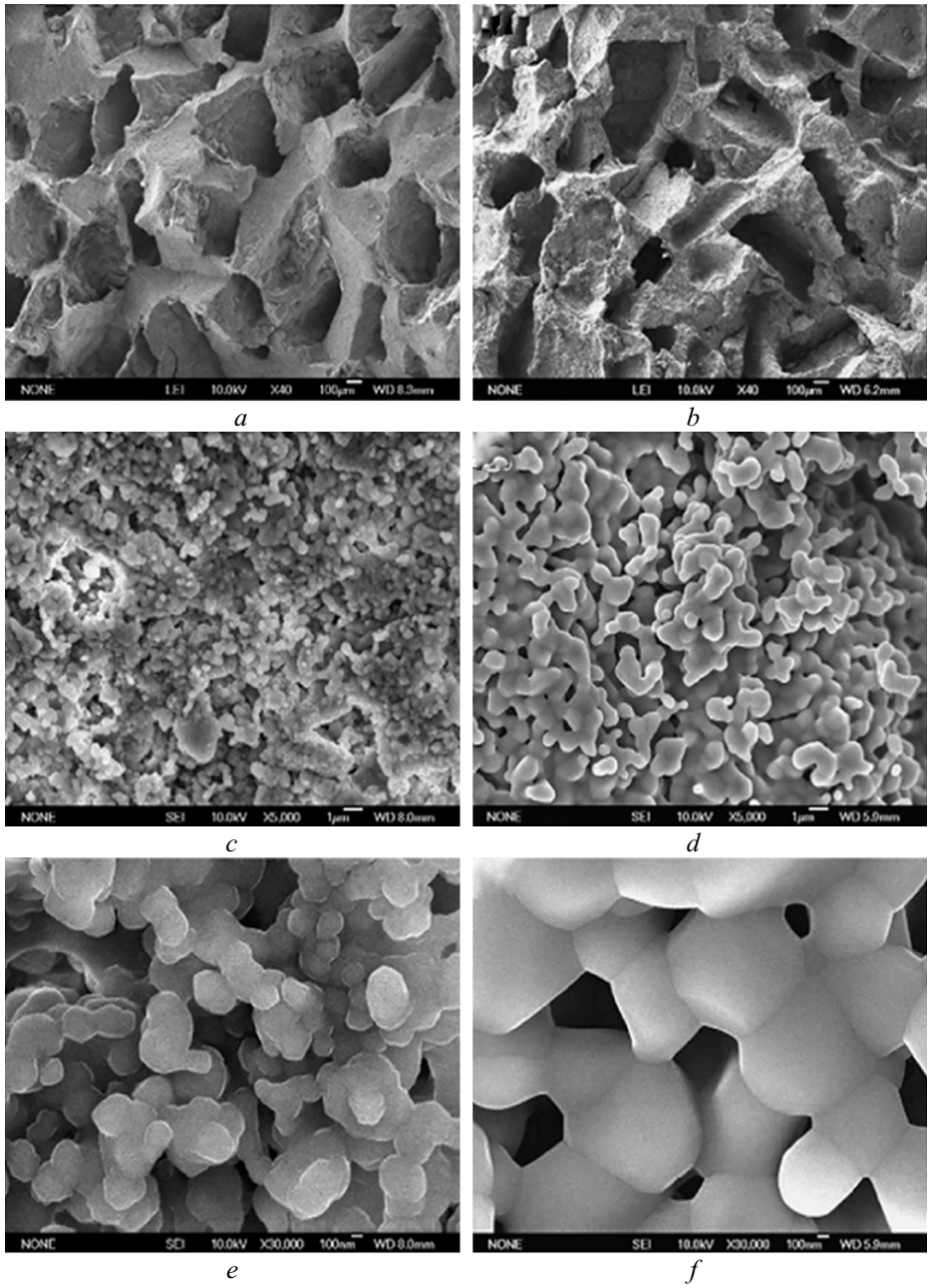

Fig. 7. SEM images of β-tricalcium phosphate scaffolds sintered by PSPS (*a*, *c*, and *e*) and conventional sintering (*b*, *d*, and *f*). Macropore sizes ranged from 300 to 500 μm, which is suitable for the osteoconduction and bone regeneration. The grain size of the scaffolds is about 200 nm and 1.0 μm for the SPS and conventionally sintered samples, respectively [63]

Figure 8 shows the samples after pellet preparation and after applying post-heat treatment at higher temperatures by PSPS. From the figure, it is clear that 700ºC is not sufficient for densification but adequate for the preparation of disk-shaped pellets with a porosity level dependent on the NaCl content in the initial powder mixture. After sintering at high temperatures, most of the micropores had disappeared and densification was ensured with no change in the pore shape due to not using pressure during SPS [64].

Two-step sintering of alumina powders by PSPS was carried out by Salamon et al. They also applied one-step sintering to elucidate the microstructure change using PSPS. Firstly, alumina powders were pressed under a pressure of 250 MPa and subjected to pressureless SPS at 1600°C for 2 min with a heating rate of 50 K/min.

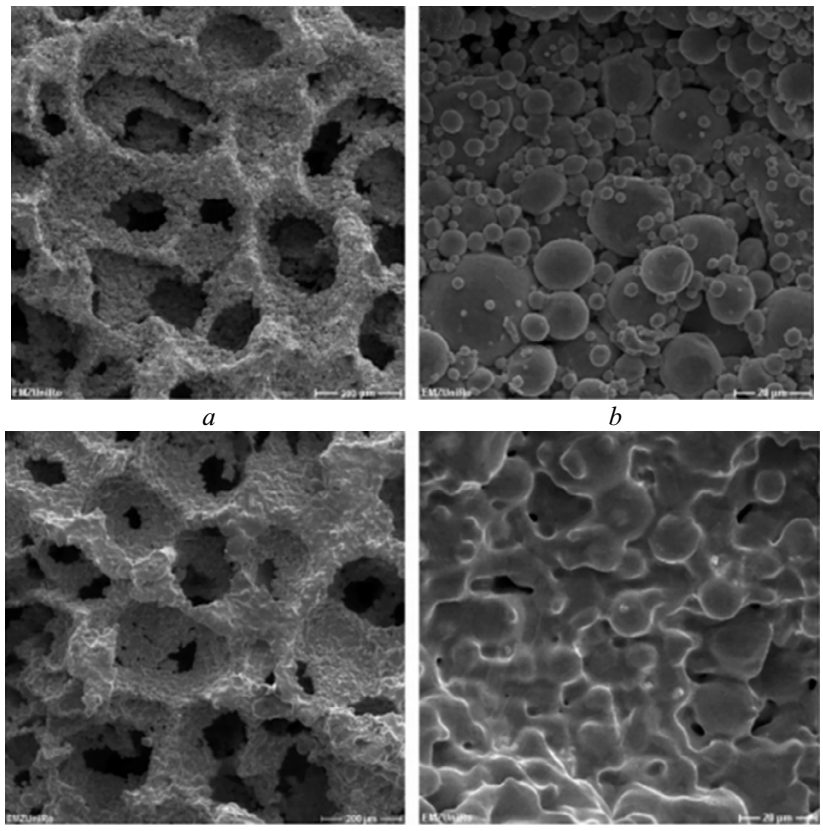

Fig. 8. SEM images of Ti_6Al_4V samples: *a*) and *b*) samples were subjected to 700°C treatment with regular SPS, *c*) and *d*) were treated at 1100°C with PSPS [64]

Secondly, as a second sintering step, the alumina compacts were regular SPS sintered at 1100ºC for 3 min with a heating rate of 100 K/min under 75 MPa pressure and then subjected to pressureless SPS sintering at 1600°C for 5 min. Their results showed that the one-step sintered sample had 95% density. After pressureless sintering at 1600°C for 2 min, grain size increased dramatically from 0.15–0.20 μm to 6.5 μm (Fig. 9*a*). For two-step sintering, the sample showed a 70% density with very fine grain size about 0.2 μm after the first stage. After the second stage, the sample had about the same density as after one-step sintering at 97%. However, the grain size was very fine and found to be as low as 2.4 μm (Fig. 9*b*) [65].

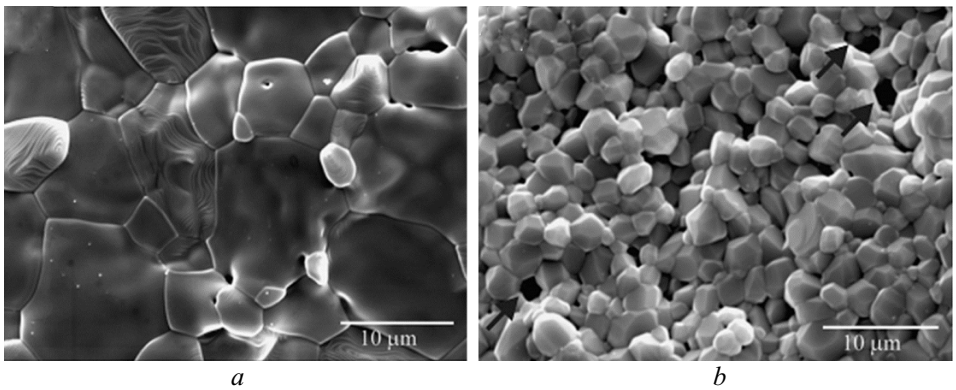

Fig. 9. SEM images of the fracture surfaces of alumina compacts: *a*) one-step PSPS at 1600°C for 2 min, *b*) two-step PSPS at 1600°C for 5 min [65]

CONCLUSIONS

In this review, we mainly focused on the various applications of PSPS in the literature. Although some PSPS applications use loose powder as a substrate, a few studies so far have used PSPS as a second step for presintered compacts. Similar to conventional SPS, the pressureless form is competitive with conventional powder metallurgical techniques. There are many different uses of PSPS, but most involve porous material production. Two different routes can be selected for the production of porous structures: using a space holder to support any applied pressure or consolidation without applying any pressure.

Usage of PSPS usually involves production of porous materials from loose powders with a modified die assembly which serves as a barrier between the loose powder and the graphite SPS die. Unlike conventional heating mechanisms, PSPS provides enhanced neck formation by applying higher heating rates, and this is one of the main advantages of regular SPS. During PSPS treatment, the chosen holding temperature and time play an important role in controlling the final porosity ratio.

In some applications of PSPS, precompacted samples are inserted in an SPS die. By using this technique, the density of the compacts can be increased by fast heating without modifying the pore or macroscale structure of the compacts. The advantage of this approach is that it provides high densification with fine grain structure due to reaching the maximum sintering temperature in a very short time.

Finally, although there has been limited research on the PSPS technique so far, this study combined many of them and discussed their results in some detail. It is clear that much like SPS treatment, PSPS will earn more attention from many researchers and will be found in many different types of applications due to the many advantages of the pressureless approach.

REFERENCES

1. C. Maniere, E. Nigito, L. Durand, A. Weibel, Y. Beynet, and E. Estournes, “Spark plasma sintering and complex shapes: The deformed interfaces approach,” *Powder Technol.*, **320**, 340–345 (2017).
2. R. Yamanoglu, E. Karakulak, and M. Zeren, “Mechanical and wear properties of prealloyed molybdenum P/M steels with nickel addition,” *J. Min. Metall. B: Metall.*, **48**, No. 2, 251–258 (2012).
3. W.D. Jones, *Fundamental Principles of Powder Metallurgy*, Edward Arnold, London (1960).
4. C.G. Goetzel, *Treatise on Powder Metallurgy: Technology of Metal Powders and Their Products*, Vol. 1, Interscience Publishers (1949).
5. P.C. Angelo and R. Submarinan, *Powder Metallurgy: Science, Technology and Applications*, PHI Learning Pvt. Ltd. (2008).
6. R.M. German, “History of sintering: empirical phase,” *Powder Metall.*, **56**, No. 2, 117–123 (2013).
7. P. Ramakrishnan, “History of powder metallurgy,” *Indian J. Hist. Sci.*, **18**, No. 1, 109–114 (1983).
8. S.Ya. Plotkin and G.L. Fridman, “History of powder metallurgy and its literature,” *Powder Metall. Met. Ceram.*, **13**, No. 12, 1026–1029 (1974).
9. R.M. German, *Sintering: from Empirical Observations to Scientific Principles*, Butterworth–Heinemann (2014).
10. R.M. German, “Sintering trajectories: description on how density, surface area, and grain size change,” *JOM*, **68**, No. 3, 878–884 (2016).
11. V.N. Chuvil’deev, M.S. Boldin, A.V. Nokhrin, and A.A. Popov, “Advanced materials obtained by spark plasma sintering,” *Acta Astronaut.*, **135**, 192–197 (2017).
12. J. Choi, H.M. Sung, K.B. Roh, S.H. Hong, G.H. Kim, and H.F. Han, “Fabrication of sintered tungsten by spark plasma sintering and investigation of thermal stability,” *Int. J. Refract. Met. Hard Mater.*, **69**, 164–169 (2017).
13. D. Salvato, J.F. Vigier, M. Cologna, L. Luzzi, J. Somers, and V. Tyrpekl, “Spark plasma sintering of fine uranium carbide powder,” *Ceram. Int.*, **43**, No. 1, 866–869 (2017).
14. S. Bahrami, M. Zakeri, A. Faeghinia, and M.R. Rahimipour, “Spark plasma sintering of silicon nitride/barium aluminum silicate composite,” *Ceram. Int.*, **43**, No. 12, 9153–9157 (2017).

15. M.M. Tünçay, J.A. Muñiz-Lerma, D.P. Bishop, and M. Brochu, “Spark plasma sintering and spark plasma upsetting of an Al–Zn–Mg–Cu alloy,” *Mater. Sci. Eng. A*, **704**, 154–163 (2017).
16. Suk-Joong L. Kang, *Sintering: Densification, Grain Growth and Microstructure*, Butterworth–Heinemann (2004).
17. R.M. German, *Sintering Theory and Practice*, John Wiley & Sons, Inc. (1996).
18. S.H. Chang and P.Y. Chang, “Study on the mechanical properties, microstructure and corrosion behaviors of nano-WC–Co–Ni–Fe hard materials through HIP and hot-press sintering processes,” *Mater. Sci. Eng. A*, **618**, 56–62 (2014).
19. R. Yamanoglu, “In situ aluminum alloy coating on magnesium by hot pressing,” *Acta Metall. Sin.*, **28**, No. 8, 1059–1064 (2015).
20. R. Yamanoglu, “Production and characterization of Al–*x*Ni in situ composites using hot pressing,” *J. Min. Metall. Sect. B: Metall.*, **50**, No. 1, 45 (2014).
21. J.E. Garay, “Current-activated, pressure-assisted densification of materials,” *Annu. Rev. Mater. Res.*, **40**, 445–468 (2010).
22. Y. Guo, H. Guo, B. Gao, X. Wang, Y. Hu, and Z. Shi, “Rapid consolidation of ultrafine grained W–30 wt.% Cu composites by field assisted sintering from the sol–gel prepared nanopowders,” *J. Alloys Compd.*, **724**, 155–162 (2017).
23. O. Guillon, J. Gonzalez-Julian, B. Dargatz, T. Kessel, G. Schierning, J. Räthel, and M. Herrmann, “Field-assisted sintering technology/spark plasma sintering: mechanisms, materials, and technology developments,” *Adv. Eng. Mater.*, **16**, No. 7, 830–849 (2014).
24. D.V. Dudina, A.G. Anisimow, V.I. Mali, N.V. Bulina, and B.B. Bokhonow, “Smaller crystallites in sintered materials? A discussion of the possible mechanisms of crystallite size refinement during pulsed electric current assisted sintering,” *Mater. Lett.*, **144**, 168–172 (2015).
25. D. Ren, Q. Deng, J. Wang, Y. Li, M. Li, S. Ran, and Q. Huang, “Densification and mechanical properties of pulsed electric current sintered B_4C with in situ synthesized Al_3BC obtained by the molten-salt method,” *J. Eur. Ceram. Soc.*, **37**, No. 15, 4524–4531 (2017).
26. Y. Kodera, C.L. Hardin, and J.E. Garay, “Transmitting, emitting and controlling light: Processing of transparent ceramics using current-activated pressure-assisted densification,” *Scr. Mater.*, **69**, No. 2, 149–154 (2013).
27. J.E. Alaniz, A.D. Dupuy, Y. Kodera, and J.E. Garay, “Effects of applied pressure on the densification rates in current-activated pressure-assisted densification (CAPAD) of nanocrystalline materials,” *Scr. Mater.*, **92**, 7–10 (2014).
28. R. Muccillo and E.N.S. Muccillo, “Light emission during electric field-assisted sintering of electroceramics,” *J. Eur. Ceram. Soc.*, **35**, No. 5, 1653–1656 (2015).
29. R. Muccillo and E.N.S. Muccillo, “Shrinkage control of yttria-stabilized zirconia during ac electric field-assisted sintering,” *J. Eur. Ceram. Soc.*, **34**, No. 15, 3871–3877 (2014).
30. Z. Liu, D. Wang, J. Li, Q. Huang, and S. Ran, “Densification of high-strength B_4C–TiB_2 composites fabricated by pulsed electric current sintering of TiC–B mixture,” *Scr. Mater.*, **135**, 15–18 (2017).
31. B. Wang, S. Zhao, F. Ojima, J.F. Yang, and K. Ishizaki, “Pulse electric current sintering of 3D interpenetrating SiC/Al composites,” *Ceram. Int.*, **43**, No. 2, 2867–2870 (2017).
32. Zuahir A. Munir, V. Quach Dat, and M. Ohyanagi, “Sintering: electric field and current effects on sintering,” *Springer*, **35**, 137–158 (2012).
33. T. Ironman, J. Tulenko, and G. Subhash, “Exploration of viability of spark plasma sintering for commercial fabrication of nuclear fuel pellets,” *Nucl. Technol.*, 1–15 (2017).
34. P. Vivekanandhan, R. Murugasami, and S. Kumaran, “Rapid in-situ synthesis of nanocrystalline magnesium silicide thermo-electric compound by spark plasma sintering,” *Mater. Lett.*, **197**, 106–110 (2017).

35. L. Zhang, Z.Y. He, Y.Q. Zhang, Y.H. Jiang, and R. Zhou, "Enhanced in vitro bioactivity of porous NiTi–HA composites with interconnected pore characteristics prepared by spark plasma sintering," *Mater. Des.*, **101**, 170–180 (2016).
36. N. Jiang, R. J. Xie, Q. Liu, and J. Li, "Fabrication of sub-micrometer MgO transparent ceramics by spark plasma sintering," *J. Eur. Ceram. Soc.*, **37**, No. 15, 4947–4953 (2017).
37. Z.A. Munir, U. Anselmi-Tamburini, and M. Ohyanagi, "The effect of electric field and pressure on the synthesis and consolidation of materials: a review of the spark plasma sintering method," *J. Mater. Sci.*, **41**, No. 3, 763–777 (2006).
38. G.F. Taylor, *US Patent No. 1,896,854* (1933).
39. G. Xie, "Spark plasma sintering: a useful technique to develop large-sized bulk metallic glasses," *J. Powder Metall. Min.*, **2**, e109 (2013).
40. A.G. Bloxam, Improved Manufacture of Electric Incandescence Lamp Filaments from Tungsten of Molybdenum or an Alloy Thereof, *GB Patent No. 190527002* (1906).
41. A.G. Bloxam, Improved Manufacture of Filaments of Tungsten or Molybdenum for Electric Incandescence Lamps. *GB Patent No. 190609020 (1906).*
42. Y. Cheng, Z. Cui, L. Cheng, D. Gong, and W. Wang, "Effect of particle size on densification of pure magnesium during spark plasma sintering," *Adv. Powder Technol.*, **28**, No. 4, 1129–1135 (2017).
43. J. Cui, L. Zhao, W. Zhu, B. Wang, C. Zhao, L. Fang, and F. Ren, "Antibacterial activity, corrosion resistance and wear behavior of spark plasma sintered Ta–5Cu alloy for biomedical applications," *J. Mech. Behav. Biomed. Mater.*, **74**, 315–323 (2017).
44. C.A. Stanciu, M. Cernea, E.C. Secu, G. Aldica, P. Ganea, and R. Trusca, "Lanthanum influence on the structure, dielectric properties and luminescence of $BaTiO_3$ ceramics processed by spark plasma sintering technique," *J. Alloys Compd.*, **706**, 538–545 (2017).
45. M. Asadikiya, C. Zhang, C. Rudolf, B. Boesl, A. Agarwal, and Y. Zhong, "The effect of sintering parameters on spark plasma sintering of B_4C," *Ceram. Int.*, **43**, No. 14, 11182–11188 (2017).
46. A. Azarniya, A. Azarniya, S. Sovizi, H.R.M. Hosseini, T. Varol, A. Kawasaki, and S. Ramakrishna, "Physicomechanical properties of spark plasma sintered carbon nanotube-reinforced metal matrix nanocomposites," *Prog. Mater. Sci.*, **90**, 276–324 (2017).
47. A. Pakdel, A. Witecka, G. Rydzek, and D.N.A. Shri, "A comprehensive microstructural analysis of Al–WC micro-and nano-composites prepared by spark plasma sintering," *Mater. Des.*, **119**, 225–234 (2017).
48. M. Bahraminasab, S. Ghaffari, and H. Eslami-Shahed, "Al_2O_3–Ti functionally graded material prepared by spark plasma sintering for orthopedic applications," *J. Mech. Behav. Biomed. Mater.*, **72**, 82–89 (2017).
49. T. Fujii, K. Tohgo, H. Isono, and Y. Shimamura, "Fabrication of a PSZ–Ti functionally graded material by spark plasma sintering and its fracture toughness," *Mater. Sci. Eng. A*, **682**, 656–663 (2017).
50. A. Teber, F. Schoenstein, F. Tetard, M. Abdellaoui, and N. Jouini, "Effect of SPS process sintering on the microstructure and mechanical properties of nanocrystalline TiC for tools application," *Int. J. Refract. Met. Hard Mater.*, **30**, No. 1, 64–70 (2012).
51. X. Yao, Z. Huang, L. Chen, D. Jiang, S. Tan, D. Michel, G. Wang, L. Mazerolles, and J.L. Pastol, "Alumina–nickel composites densified by spark plasma sintering," *Mater. Lett.*, **59**, No. 18, 2314–2318 (2005).
52. R. Yamanoglu, W. Bradbury, E. Karakulak, E.A. Olevsky, and R.M. German, "Characterization of nickel alloy powders processed by spark plasma sintering," *Powder Metall.*, **57**, No. 5, 380–386 (2014).
53. G. Antou, P. Guyot, N. Pradeilles, M. Vandenhende, and A. Maître, "Identification of densification mechanisms of pressure-assisted sintering: application to hot pressing and spark plasma sintering of alumina," *J. Mater. Sci.*, **50**, No. 5, 2327–2336 (2015).
54. Yann Aman, Vincent Garnier, and Elisabeth Djurado, "Pressureless spark plasma sintering effect on non-conventional necking process during the initial stage of sintering of copper and alumina," *J. Mater. Sci.*, **47**, No. 15, 5766–5773 (2012).

55. William L. Bradbury and Eugene A. Olevsky, “Production of SiC–C composites by free-pressureless spark plasma sintering (FPSPS),” *Scr. Mater.*, **63**, No. 1, 77–80 (2010).
56. D. Giuntini, X. Wei, A.L. Maximenko, L. Wei, A.M. Ilyina, and E.A. Olevsky, “Initial stage of free pressureless spark-plasma sintering of vanadium carbide: Determination of surface diffusion parameters,” *Int. J. Refract. Met. Hard Mater.*, **41**, 501–506 (2013).
57. L. Bertolla, I. Dlouhý, P. Tatarko, A. Viani, A. Mahajan, Z. Chlup, M. Reece, and A.R. Boccaccini, “Pressureless spark plasma–sintered Bioglass® 45S5 with enhanced mechanical properties and stress–induced new phase formation,” *J. Eur. Ceram. Soc.*, **37**, No. 7, 2727–2736 (2017).
58. Dina V. Dudina, Boris B. Bokhonov, and Amiya K. Mukherjee, “Formation of aluminum particles with shell morphology during pressureless spark plasma sintering of Fe–Al mixtures: current-related or Kirkendall effect?” *Materials*, **9**, No. 5, 375 (2016).
59. R. Yamanoglu, N. Gulsoy, E.A. Olevsky, and H.O. Gulsoy, “Production of porous Ti5Al2.5Fe alloy via pressureless spark plasma sintering,” *J. Alloys Compd.*, **680**, 654–658 (2016).
60. Rachman Chaim, “Liquid film capillary mechanism for densification of ceramic powders during flash sintering,” *Materials*, **9**, No. 4, 280 (2016).
61. J. Meng, N.H. Loh, B.Y. Tay, S.B. Tor, G. Fu, K.A. Khor, and L. Yu, “Pressureless spark plasma sintering of alumina micro-channel part produced by micro powder injection molding,” *Scr. Mater.*, **64**, No. 3, 237–240 (2011).
62. Y.S. Lin, M.A. Meyers, and E.A. Olevsky, “Microchanneled hydroxyapatite components by sequential freeze drying and free pressureless spark plasma sintering,” *Adv. Appl. Ceram.*, **111**, Nos. 5–6, 269–274 (2012).
63. F. Zhang, K. Lin, J. Chang, J. Lu, and C. Ning, “Spark plasma sintering of macroporous calcium phosphate scaffolds from nanocrystalline powders,” *J. Eur. Ceram. Soc.*, **28**, No. 3, 539–545 (2008).
64. Y. Quan, F. Zhang, H. Rebl, B. Nebe, O. Keßler, and E. Burkel, “Ti6Al4V foams fabricated by spark plasma sintering with post-heat treatment,” *Mater. Sci. Eng. A*, **565**, 118–125 (2013).
65. David Salamon and Zhijian Shen, “Pressureless spark plasma sintering of alumina,” *Mater. Sci. Eng. A*, **475**, No. 1, 105–107 (2008).